

Optical Observation of Neutral Beam Attenuation in Hydrogen Discharge at LHD

Katsunori IKEDA, Masaki OSAKABE, Allan WHITEFORD¹⁾, Katsumi IDA, Osamu KANEKO, Daiji KATO, Shigeru MORITA, Kenichi NAGAOKA, Yasuhiko TAKEIRI, Katsuyoshi TSUMORI, Masayuki YOKOYAMA, Mikiro YOSHINUMA, and LHD experiment group

National Institute for Fusion Science, Toki, Gifu 509-5292, Japan

¹⁾*University of Strathclyde, 107 Rottenrow Glasgow, UK*

(Received: 4 September 2008 / Accepted: 10 February 2009)

Hydrogen Balmer light emissions from a high energy neutral beam have been observed in a hydrogen discharge plasma at the Large Helical Device. At beginning of the additional high energy neutral beam heating, we have observed strong beam attenuation with a peak electron density profile. Then the signal of beam emission intensity increases at the downstream position, namely passing neutral beam particles increase, when the electron density become to hollow distribution. We have calculated a beam stopping coefficient along the beam injection axis used the Atomic Data and Analysis Structure (ADAS) code. An ionized neutral beam in the peak density distribution is 11% larger than that in the hollow density distribution. We also checked a beam emission flux reconstructed by the beam stopping coefficient and the beam emission coefficient. The time evolution of beam emission flux is consistent to the measured beam emission signals.

Keywords: neutral beam, beam mission, attenuation, ADAS, LHD

1. Introduction

A neutral beam injector (NBI) is a useful device to increase ion heating power for fusion device. In the Large Helical Device (LHD), three high-energy ($E = 180\text{keV}$) NBIs used two negative ion sources [1] and a low-energy ($E = 40\text{keV}$) NBI used four positive ion sources [2] operate now. High-energy neutral beams are injected tangentially as shown in Fig. 1. It was well performed to increase the ion temperature to $T_i = 13\text{keV}$ in the argon discharge plasma with low electron density ($n_e < 1 \times 10^{19}\text{m}^{-3}$) due to the increasing direct heating power [3, 4]. In a hydrogen discharge, ion temperature was increased around 2keV used only the high energy NBI which heats plasma electrons dominantly. It is important to understand the characteristics of the NBI heating with high energy beam for future NBI system such as in ITER (International Thermonuclear Experimental Reactor) [5]. To investigate the beam absorption, we have installed a visible spectroscopy system to observed the hydrogen spectrum from the neutral beam along the beam injection axis.

In the following, we present the beam emission signals at a upstream position and a downstream position in the hydrogen discharge plasma at LHD. Beam stopping coefficients along the beam injection axis estimated by a radial electron density profile. Then we will discuss a beam deposition from the comparison of the reconstruction beam emission flux and the mea-

sured beam emission signal.

2. Beam Emission Diagnosis

Figure 1 shows the schematic top view of the LHD with four NBIs. Two hydrogen negative ion sources called IS-3A and IS-3B are installed in the third beam line (BL3), and each beam is tilted 1.8° from the beam injection axis in order to pass the injection port. To investigate neutral beam attenuation, we set two optical sight lines along the beam injection axis[6] as also shown in Fig 1. The quartz optical fibers with a small lens viewing the upstream position and the downstream position are set at the 6-o port and the 5-o port with the angle of 62.4° and 134.7° from the beam injection axis, respectively. We have arranged a 25cm Czerny-Turner spectrometer with a grating of 1800grooves/mm at the end of the optical fiber. An intensified charge couple device (ICCD) detector cooled down -20°C is attached on the focal plane of the spectrometer, and the spectral resolution 0.21nm in totally. Hydrogen Balmer- α spectrum ($\text{H}\alpha$) with the wavelength of 656.3nm is emitted from plasma discharge with isotropic distribution and from neutral beams due to the interaction of beam and plasma particles. We can separate the background $\text{H}\alpha$ spectrum and the beam emission $\text{H}\alpha$ spectrum which is shifted by Doppler effect due to the speed of neutral beam particles. The beam emissions from the upstream position and the downstream position are also separated due to the opposite direction of two sight lines. A time resolution of ICCD detector depend on an expo-

author's e-mail: ikeda.katsunori@lhd.nifs.ac.jp

sure time and a read out time, here we use the 20ms exposure time and the 40ms interval time for frame sampling. To compare the beam emission intensity between the two positions, the spectrometer system included the ICCD detector and optical fibers is calibrated by an Urbright sphere with a standard lamp.

3. Neutral Beam Attenuation in Hydrogen Plasma

Figure 2 shows the time evolution of hydrogen discharge used NBI heating, here the center magnetic field strength is $B = 2.769T$ and the major radius is $R_{ax} = 3.575m$. This plasma is built up by an electron cyclotron resonant heating during $t = 0.3s$ to $t = 0.6s$, and is sustained by the 40keV low energy neutral beam from $t = 0.5s$ used fourth beam line (BL4). The averaged electron density measured by a far infrared ray (FIR) laser interferometer is increased to $\langle n_e \rangle = 2 \times 10^{19}m^{-3}$ as shown in Fig. 2(b). Additional 13MW neutral beams from the first beam line (BL1), second beam line (BL2) and BL3 are injected after $t = 0.9s$, here the beam energy of BL1, BL2 and BL3 is 170keV, 182keV and 167keV respectively. The stored energy W_p increase by the additional beam heating as shown in Fig. 2 (b). The ion temperature measured by the Doppler broadening of ArXVII spectrum from impurity argon increases to 2.5keV which is similar behavior of the electron temperature measured by the Thomson scattering as shown in Fig.2 (c).

Figure 2(d) shows the time evolution of beam emission H α intensity from the neutral beam of BL3. Circle marks and square marks are the line integral light emissions measured at the upstream position and the downstream position, respectively. At the beginning of the beam injection, the beam emission intensity at the downstream sight is half of the intensity which is observed at the upstream sight. Though the averaged electron density is almost constant shown in Fig. 2(b), the increasing of the beam emission signal has been observed during $t = 1.0s$ to $t = 1.43s$ at the downstream position. The beam emission flux $\Phi(L)$ is expressed as follows [7];

$$\Phi \propto n_e(L)\epsilon_{cr}(L)n_{beam}(L), \quad (1)$$

where $n_e(L)$ and $\epsilon_{cr}(L)$ is an electron density and an emission coefficient, respectively, $n_{beam}(L)$ is a neutral beam density attenuated as far as the position of L along the injection axis. From the result of the beam emission, it is thought that strong beam deposition occurs at the beginning of additional beam injection.

We also have found a difference on the density distribution obtained by the Thomson scattering system calibrated by the FIR interferometer as shown in Figure 3(a). The electron density distribution forms a peak distribution due to the increasing center parti-

cle supply after the additional tangential beam injection expressed as circle marks with the center electron density about $n_e = 2 \times 10^{19}m^{-3}$ at $t = 1.0s$, when the minimum beam emission is observed at the downstream position. Then the center electron density decreases to $n_e = 1.2 \times 10^{19}m^{-3}$ with the hollow density distribution at $t = 1.43s$. This transformation of density distribution is not controlled, and it might occur by the increasing of recycling particles from vacuum chamber wall and diverter plates. The center electron temperature T_e measured by the Thomson scattering system forms almost same distribution during the discharge as shown in Fig. 3(b).

To investigate a relationship between beam deposition and the density distribution, we have calculated a beam attenuation factor along the beam injection axis. Figure 4 shows the attenuation parameters along the beam injection axis from IS-3A, here the horizontal axis L is the length of beam running from the ion source. The beam penetration length is about 5m long due to the tangential beam injection. Neutral beam passes through more dense plasma at $t = 1.0s$ expressed the circle mark with the peak distribution than the density in the hollow distribution expressed the square mark and the triangle marks in Fig. 4(a). The beam stopping coefficient S_{cr} for hydrogen target plasma with peak density evaluated by the Atomic Data and Analysis Structure (ADAS) [8, 9] is also large values in most places along the beam injection axis at $t = 1.0s$ as shown in Fig. 4(b). Hence the deposition neutral beam power increases in the case of peak density. We have defined the beam attenuation factor $n_{beam}(L)/n_{beam}(P)$ as follows;

$$\frac{n_{beam}(L)}{n_{beam}(P)} = \exp\left(-\int_P^L n_e(l)S_{cr}(l)\sqrt{\frac{m}{2E}}dl\right), \quad (2)$$

where the $n_{beam}(L)$ is the local neutral beam density at L , $n_{beam}(P)$ is the neutral beam density path through the beam injection port at the position of P , $n_e(l)$ is the local electron density, $S_{cr}(l)$ is the local stopping coefficient, m is the mass of the beam particle and E is the beam energy. The neutral beams approximately decrease to 50 ~ 60% before the upstream position where is the nearest position to the torus center as shown in Fig. 4(c), here the dotted lines are the observation points. Then about 75% of the neutral beams are deposited in the hydrogen plasma with the peak density distribution at the downstream position. The difference of the attenuation factor between the peak density case and the hollow density cases is expanded to 11% at the end of beam penetration.

Using the attenuation factor, we have estimated the time evolution of the beam deposition power as shown in Fig. 5(a). The maximum deposition rate is 75% at $t = 1.0s$ with peak density, but it decreases to 65% at $t = 1.43s$ with hollow density. Cross marks are

the port through power obtained by the power supply parameters and the calorimetric measurement on the beam armor tiles. The deposition power evaluated by the product of the port through power and the deposition rate increases to 2.6MW at $t = 1.0\text{s}$, but it decreases to 2.3MW at $t = 1.43\text{s}$ with hollow density distribution. From this result, peak density distribution has contributed to increase heating neutral beam power in totally.

To confirm the beam attenuation factor, we have estimated $\text{H}\alpha$ beam emission flux from the beam attenuation factors these are shown at the dotted lines in Fig. 4(c) and the beam emission coefficient $\epsilon_{cr}(L)$ calculated by the ADAS analysis with the same procedure of the beam stopping coefficient. From the relation of the Equation 1, we have calculated the beam emission flux as a relative value as follows; $\Phi(L) = n_e(L)\epsilon_{cr}(L)P_{beam}(P)n_{beam}(L)/n_{beam}(P)$, here $P_{beam}(P)$ is the port through power. The dotted line and the bold line plotted in Fig. 5(b) is reconstructed photon flux, which includes two beam components (i.e. IS-3A and IS-3B), at the upstream position and the downstream position, respectively. At the upstream position, the beam emission flux dose not so change during discharge, because the difference of penetrate n_{beam} is canceled by the difference of center n_e between $t = 1.0\text{s}$ and $t = 1.43\text{s}$. At the downstream position, however, the attenuation factor 0.25 at $t = 1.0\text{s}$ increase to 0.36 at $t = 1.43\text{s}$ as shown in Fig 4(c). The difference of attenuation factor 0.11 is large enough to increase beam emission flux Φ with the small changing of $n_e(L)$ at downstream. Therefore the beam attenuation is more clearly observed at the downstream position.

In conclusion, a weak $\text{H}\alpha$ beam emission has been observed in the hydrogen discharge plasma due to the strong beam attenuation with the peak n_e distribution at the downstream position. The beam stopping coefficient in the peak density profile along the beam injection axis calculated by the ADAS analysis is larger than that in the hollow density distribution. Behavior of reconstruction beam emission flux is good agreement with measured beam emission signals.

ACKNOWLEDGMENTS

The authors would like to thank the LHD and NBI staff for their operational and diagnostic support. They would like to thank Prof. T. Kato and Prof. I. Murakami (National Institute for Fusion Science), and Prof. H. Summers (University of Strathclyde) for useful discussions. This work is supported by NIFS/NINS under the project of Formation of International Network for Scientific Collaborations. This work is also supported by the budget for NIFS08ULBB517.

References

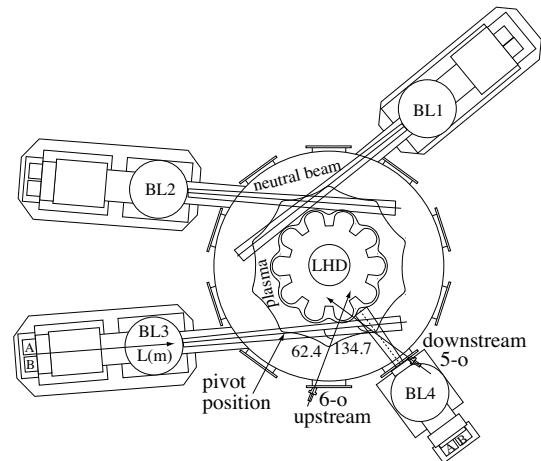


Fig. 1 Schematic top view of the LHD and neutral beam injectors. Two optical sight lines to measure hydrogen beam emission light is set at the upstream position and the downstream position.

- [1] Y. Takeiri, O. Kaneko, K. Tsumori *et al.*, Nucl. Fusion **46** S199 (2006).
- [2] K. Nagaoka, K. Ikeda, M. Osakabe *et al.*, Plasma and Fusion Research **2** S1051 (2007).
- [3] K. Ikeda, M. Osakabe, Y. Takeiri *et al.*, Journal of the Korean Physical Society **49** (6) S96-S99 (2006).
- [4] Y. Takeiri, S. Morita, K. Ikeda *et al.*, Nucl. Fusion **47** 1078 (2007).
- [5] R. S. Hemsworth, J.-H. Feist, M. Hanada *et al.*, Rev. Sci. Instrum. **67**, 1120 (2007).
- [6] K. Ikeda, M. Osakabe, A. Whiteford *et al.*, Transactions of Fusion Science and Technology **51** (2T), 283-285, (2007).
- [7] W. Mandl, R. C. Wolf, M. G. von Hellermann and H. P. Summers, Plasma Phys. Control. Fusion **35** 1373 (1993).
- [8] H. Anderson, M. G. von Hellermann, R. Hoekstra *et al.*, Plasma Phys. Control. Fusion **42**, 781 (2000).
- [9] H. P. Summers, H. Anderson, T. Kato and S. Murakami, Research Report NIFS-DATA Series No. 55, Nagoya, November (1999).

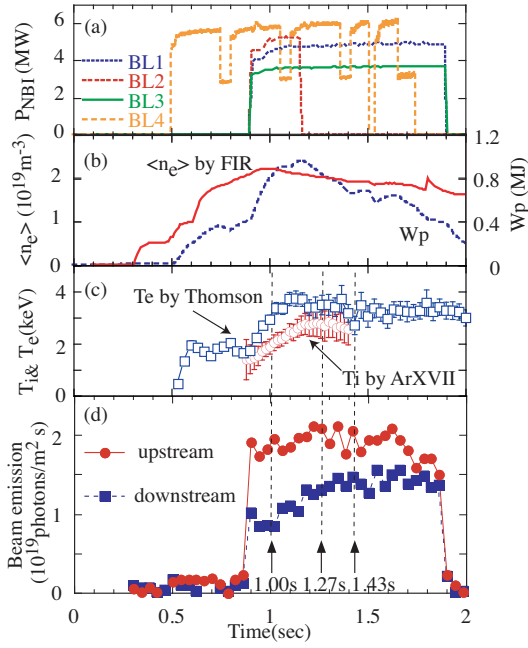


Fig. 2 Time evolutions of injected neutral beam powers (a), the line averaged n_e and stored energy W_p (b), the T_i and T_e (c), and the beam emission intensities at upstream and downstream (d).

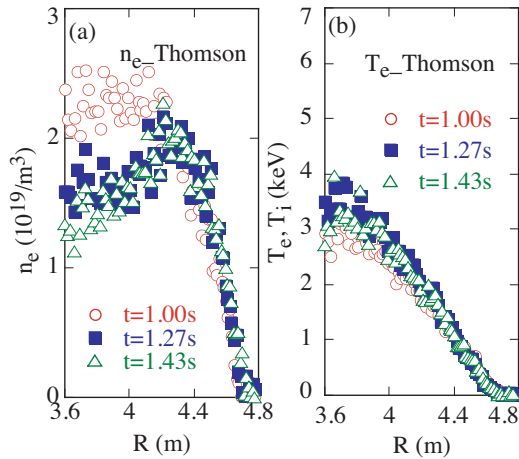


Fig. 3 Outer half radial profiles of n_e (a) and T_e (b) by Thomson scattering. n_e profile is calibrated by $\langle n_e \rangle$.

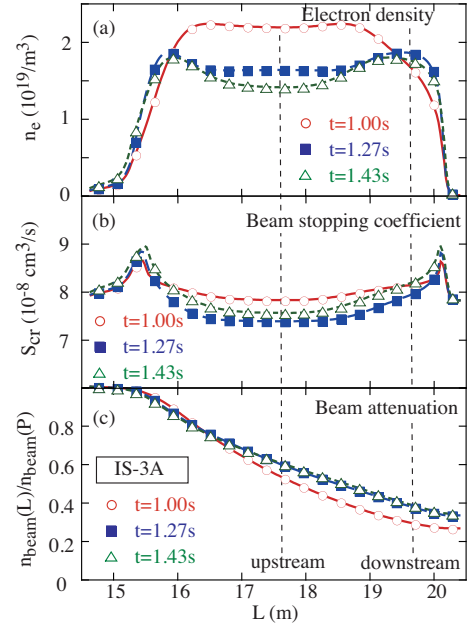


Fig. 4 Along the beam injection axis of IS-3A, the distribution of n_e (a), and the beam emission coefficient obtained by ADAS data (b), and the neutral beam attenuation factor (c) with the peak density distribution (circle marks) or the hollow density distribution (square marks and triangle marks). Dotted lines are the observed positions at the upstream and the downstream

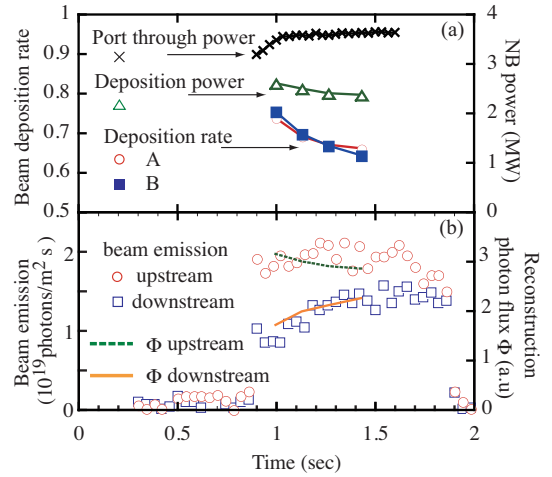


Fig. 5 Time evolution of the beam deposition power obtained by the beam attenuation rate and the port through power (a). Photon fluxes of the beam emission at upstream position (dotted line) and downstream position (bold line) reconstructed by the beam attenuation rate and the beam emission coefficient are plotted on the measured beam emission intensities (b).